PROCEEDINGS, TOUGH Symposium 2012
Lawrence Berkeley National Laboratory, Berkeley, California, September 17-19, 2012

NUMERICAL SIMULATION OF DNAPL SOURCE ZONES ABOVE AND BELOW THE WATER TABLE IN FRACTURED SANDSTONE

Ken Walton[1], Andre Unger, Mario Ioannidis, and Beth Parker

[1]Department of Earth and Environmental Sciences, University of Waterloo
200 University Avenue West
Waterloo, Ontario, N2L3G1, Canada
e-mail: kmwalton@uwaterloo.ca

ABSTRACT

Numerical simulation of flow of two or three mutually interactive phases is a standing challenge for model developers and practitioners. Applying such flow models in the context of fractured rock, an extreme case of heterogeneity, further increases the complexity of the problem. Depending on the rigor of the coupling of flow and transport equations and the geometric description of the fractured-rock domain, problems such as these quickly become at best computationally burdensome, and at worst completely intractable.

In this paper, we describe a mesh generator that spatially discretizes a porous medium and network of discrete, orthogonal fractures and provides influence coefficients for fracture-fracture, matrix-matrix, fracture-matrix, and asperity contact-bridged matrix-matrix flow. We demonstrate an application of this non-uniform spatial mesh in the numerical model *CompFlow Bio* (a multi-component, three-phase flow and transport simulator) in the real-world context of the Santa Susana Field Laboratory site (a site of trichloroethylene (TCE) contamination in fractured sandstone). We provide demonstration simulations of TCE source evolution via a series of three simulations: two smaller-scale (~10 m) air/water/TCE simulations in a near-surface zone; and one larger-scale (~100 m) water/TCE simulation below the water table. The physical processes we consider are capillary barriers to water and TCE flow in the vadose zone, asperity contact bridged flow, and fast preferential flow in the fracture network. All of these processes are parameterized in the model by quantities that could be derived from real site data. Finally, we touch on the computational burden of these various scenarios and contrast meshes of this scheme to conventional finite volume grids.

INTRODUCTION

Numerical modeling of two- and three-phase flow is relevant in fields of carbon sequestration, radionuclide storage, petroleum reservoir production, and (as is our focus) contaminant hydrogeology. These fields seek to predict how distinct fluid phases flow and interact within geologic media. The presence of heterogeneity, be it from differences in rock or soil type, local variations in rock or soil characteristics, or the presence of fractures with varying orientation and aperture, complicate the physical description of the domain of interest and increase the computational burden of numerical simulators, a tool commonly used by practitioners.

These tools, their conceptual design and implementation, unite knowledge from chemistry, fluid mechanics, geology, applied mathematics, and computer science. Here, we omit many relevant details from these fields as we elaborate only on our geometric description of discrete fractures, and show numerical simulations that act as examples of its use in the numerical model *CompFlow Bio* (see e.g., Unger et al., 1995). The ultimate goal of our geometric description is to produce “influence coefficients” (blended spatial and geophysical values that quantify the degree to which adjacent computational entities interact) suitable for a finite volume discretization scheme. Herein, we highlight the major concepts behind our approach, including (1) our motivation to consider fractures as distinct computational entities, (2) our notion of a discrete fracture with asperity contact area, (3) the procedure for addition of fractures into the spatial mesh as control volumes (CVs), and (4) the advantageous step of eliminating small-volume CVs that occur at the intersection of fractures. We then briefly describe some

simulation results and discuss pros and cons of this method.

METHOD

Motivation

First, we examine our choice of the discrete fracture conceptual model: We take the pedagogical assumption that small-scale flow and transport phenomena (when upscaled appropriately) contribute to the overall flow field, and that a statistically generated fracture network based on field measurements represents the actual fracture network sufficiently well. Furthermore, we assume that discrete fractures have three-phase relative permeability-saturation-capillary pressure (k_r-S-P_c) relationships (similar to porous media, as per Reitsma and Kueper, 1994) that are an important aspect of their influence on multiphase flow.

Figure 1 shows a complex pattern of aqueous phase and nonaqueous phase saturation that may arise from fracture-matrix interactions. Capillarity causes fractures to be gas-filled and act as barriers to liquid flow; areas where opposing fracture walls are in contact relieve these barriers.

Discrete Fracture Conceptualization

We consider individual rough fractures, such as in Figure 2(a), to be composed of one or more component CVs, which are distinct computational entities in the simulator. Fracture CVs are much like porous media CVs, except that they have porosity 1.0, they have fewer than three spatial dimensions (i.e. they are planar as in Figure 2(b), or in the case of fracture intersections, are one- or zero-dimensional). Moreover, their intrinsic permeability tensor is limited by the dimensionality of the CV, permeability is calculated according to the cubic law using effective hydraulic aperture, and they hold their own set of k_r-S-P_c relationships.

Fracture CVs may connect to other fractures at their edges and adjacent porous medium (or rock matrix) CVs over their faces. We augment connectivity by allowing direct matrix-to-matrix flow across a fracture plane by asperity contact-bridged flow; we assume the porous media at contact points to be continuous and that regular

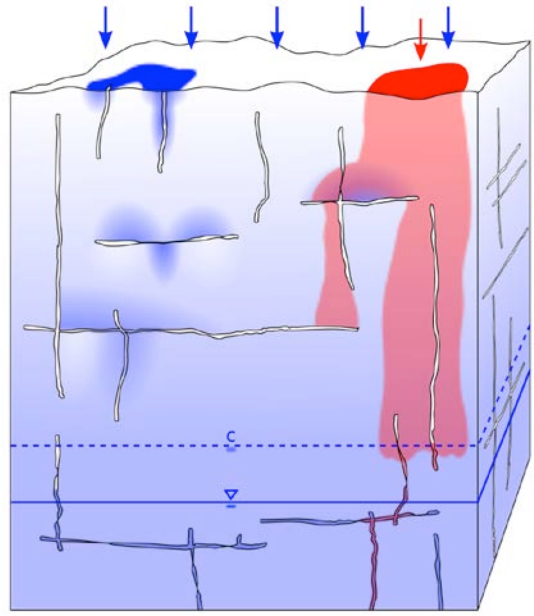

Figure 1. Schematic of how discrete fractures may influence fluid phase saturation in the vadose and shallow saturated zones, given infiltrating aqueous phase (blue), non-aqueous phase contaminant (red), and a resident gas phase (white).

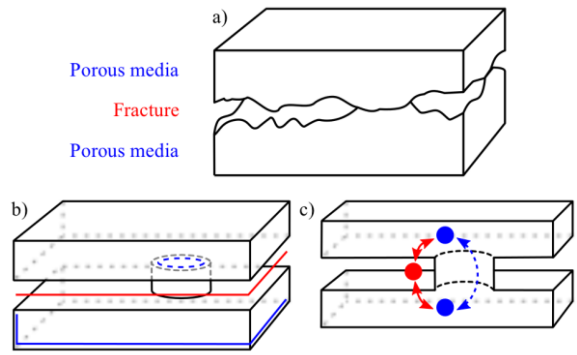

Figure 2. (a) Conceptual diagram of a rough fracture, (b) dimensions of 2D fractures and 3D porous media CVs, and (c) fracture-matrix and matrix-matrix connectivity.

Darcy flow occurs through these areas. Thus, a fraction, $0.0 \leq \alpha \leq 1.0$, of each planar fracture CV's area is allocated for such flow, as depicted conceptually in Figure 2(c).

Spatial Discretization

For the purpose of reducing the overall number of control volumes in the domain, porous media CVs are refined only in areas local to fractures. This is accomplished in a mesh preprocessing step whereby the fractures are added one by one

to an initial grid of porous media CVs. Porous media blocks are bisected in the plane of the fracture, but not necessarily at the edges of the fracture. This is different from a conventional finite volume or finite element discretization, in which the boundaries of fractures or adjacent CVs/elements always coincide. Fractures are subdivided into CVs based on the boundaries of surrounding CVs.

For example, in Figure 3, the porous medium block A is split into A' and A" to accommodate C. B remains unchanged. Connectivity is rees-tablished based on the interfacial areas of CVs in contact with one another.

We note that the resulting mesh lacks the original well-defined grid-like structure. The boundaries of adjacent CVs are often mis-aligned, as Figure 3 indicates. This misalign-ment is an extra source of numerical inaccuracy in the solution of flow and transport equations (Dehotin et al., 2011). We feel that the trade-off of reduced accuracy in order to reduce the overall number of CVs is warranted.

Numerical Formulation

Once the CVs and connectivity relationships have been established, the next step is to quantify those relationships for flow and transport.

To illustrate how to calculate interfacial areas and influence coefficients in an irregular mesh formed by the process above, we present Figure 4. In this situation, typical of relatively large initial porous media CVs bisected by randomly spaced fractures, the boundaries of porous media CVs, *i* and *j*, are disjointed, and the fracture CV,

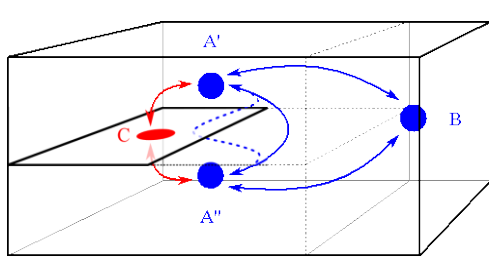

Figure 3. Adjacency relationships of fracture-matrix (red) and matrix-matrix (blue) CVs, including an asperity contact connection between A' and A" (blue, dashed).

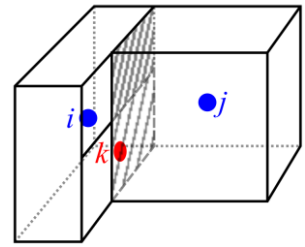

Figure 4. An example of adjacent porous media CVs, *i* and *j*, and fracture CV *k* with disjointed boundaries.

k, lies between them. The dark gray area of direct contact between *i* and *j* plus the light gray area times the asperity contact fraction com-prises the entire interfacial area.

Influence coefficient calculation

Influence coefficients in *CompFlow Bio* are calculated in a typical way for finite volume dis-cretizations. Interfacial area is multiplied by a weighted average of permeabilities, and divided by the distance between the node centroids. For example:

$$\gamma_{ij} := A_{ij} \frac{k_{II,i} k_{II,j} \left(\Delta x_{I,i} + \Delta x_{I,j}\right)}{k_{II,j} \Delta x_{I,i} + k_{II,i} \Delta x_{I,j}} \left(\frac{\Delta x_{I,i} + \Delta x_{I,j}}{2}\right)^{-1}$$

where *i* and *j* are CV labels, A_{ij} is the interfacial area between *i* and *j*, $k_{II,i}$ is the intrinsic perme-ability of node *i*, entry *I*-*I* of the 3×3 tensor, and $\Delta x_{I,i}$ is the size (or aperture) of node *i* in direc-tion principle Cartesian direction *I*. (We note that the above formula could be replaced with an equation from the literature to accommodate a permeability tensor that is not aligned with the principle Cartesian vectors. Because our fractures and porous media CV faces are aligned with the axes, this is not necessary.)

Intersection Node Elimination

Although fracture intersections may be important preferential pathways in multiphase flow, we eliminate these CVs from the mesh to ease the numerical burden they impose. (This is a necessary step for "large" simulations; inter-sections can be retained otherwise.) Elimination occurs in a post-processing step, in which new connectivity and influence coefficients are formed. These influence coefficients arise from algebraic manipulation of the steady-state flow

equation at the eliminated node. Thus, some information/effect of the node is retained.

Node elimination occurs in two stages: Point intersections are removed, then line intersections are removed. Influence coefficients are calculated at each iteration, as they are all used in forming subsequent coefficients.

Figure 5 shows the CVs representing the fracture planes and intersections in a situation where three fractures meet in a corner-like configuration.

Influence coefficient calculation for control volume elimination

Taking the *E-F* connection in Figure 5 as an example, the influence coefficient, which uses information from former neighbors of *b*, is given by:

$$\gamma''_{EF} := \frac{\gamma_{bE}\gamma_{bF}}{\sum_{j\epsilon\eta_b}\gamma_{bj}}$$

$$= \frac{\gamma_{bE}\gamma_{bF}}{\gamma_{bE}+\gamma_{bF}+\gamma'_{bc}+\gamma'_{bd}}$$

$$= \frac{\gamma_{bE}\gamma_{bF}}{\gamma_{bE}+\gamma_{bF}+\frac{\gamma_{ab}\gamma_{ac}}{\gamma_{ab}+\gamma_{ac}+\gamma_{ad}}+\frac{\gamma_{ab}\gamma_{ad}}{\gamma_{ab}+\gamma_{ac}+\gamma_{ad}}}$$

where η_b is the set of neighbors of node *b*, γ'_{bc} and γ'_{bd} are defined in-place, and other unprimed γs are defined in the previous equation.

APPLICATION

As a demonstration of this mesh creation approach and examples of the scale of the problem it is being employed to tackle, we present the sample meshes and results of three simulations conducted with *CompFlow Bio*.

The simulation scenario is based on subsurface contamination at the Santa Susana Field Laboratory site, located near Los Angeles, California. To investigate dense, nonaqueous phase liquid (DNAPL) source zone architecture, DNAPL is introduced at the ground surface and allowed to infiltrate downward through the vadose zone, capillary fringe, and below the water table. We consider gravity-driven gas, aqueous phase, and NAPL flow, capillarity, equilibrium phase partitioning, and dissolved species transport. Gas exchange and steady recharge occur at the top of the domain, while

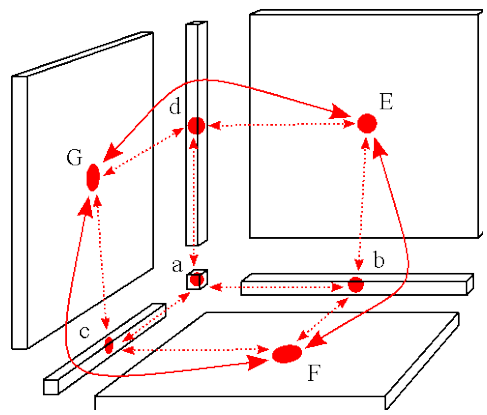

Figure 5. Neighbor relationships between fracture CVs at the intersection of three orthogonal fractures before and after node elimination. CVs are separated spatially for clarity.

hydrostatic, free-flow conditions exist at the bottom. The rock matrix properties, such as permeability and k_r-S-P_c relationships, are homogeneous. Fracture spacing is approximately 3 per meter (or 1 per meter in the 3D, saturated simulation) and fracture aperture varies log-normally with mean aperture 150 µm. Wherever possible, simulation parameters are derived from measurements of the fractured Chatsworth formation sandstone taken from the site. DNAPL loading occurs in a small area at the top of the domain at a steady rate of 7 L/day (or about one 55 gallon drum per month) in each case.

Figures 6, 7, and 8 show transient DNAPL source zones at various points in time. They also demonstrate the density of the fracture network, and complicated architecture that ensues from the contributions of distinct fracture and matrix CVs.

To provide a basic description of the certain computational costs, characteristics of the meshes in the preceding simulations are provided in Table 1. These data are highly implementation- and random-fracture-network-dependent, but nonetheless provide a baseline for comparison to simulations from other platforms. For further comparison, we give values for analogous meshes generated in the conventional fashion: we take the same fracture networks and a priori impose grid lines in the plane of each fracture.

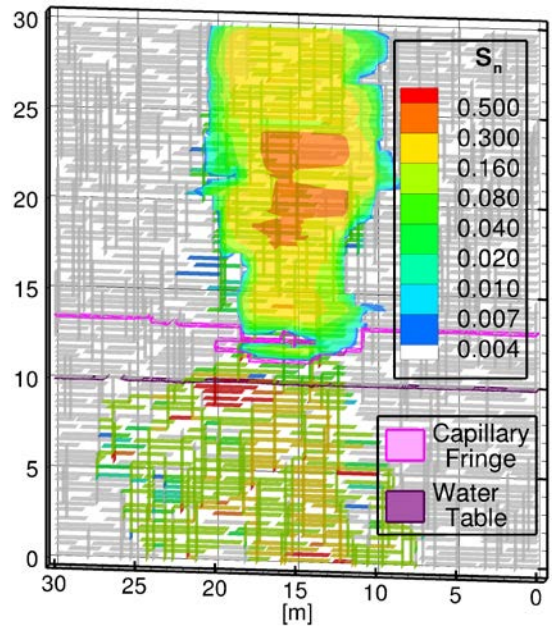

Figure 6. DNAPL saturation after 2 years of contaminant loading in a 30×1×30 m domain.

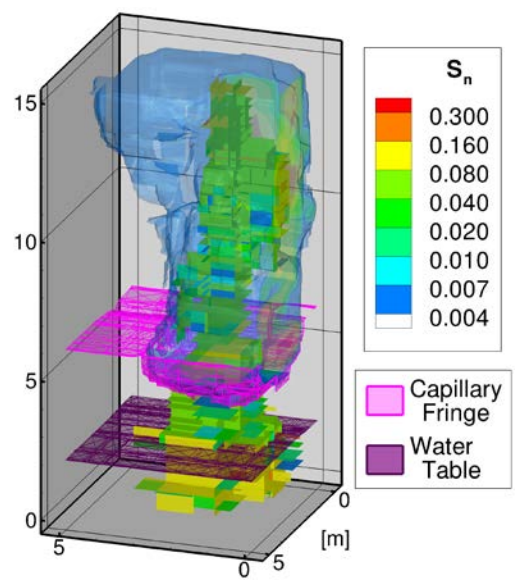

Figure 7. DNAPL saturation after 1 year of contaminant loading in a 5×5×15 m domain. Fracture CVs with low DNAPL saturation omitted.

DISCUSSION

To support the modeling of three-phase flow in fractured media, we have presented a framework for creating a spatial mesh which (1) reduces the number of CVs, and (2) removes numerically troublesome, small-volume CVs. As evidence that the approach is viable, we presented results

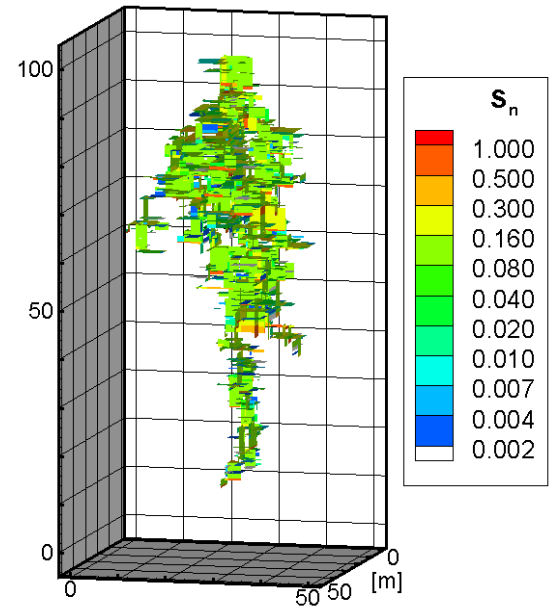

Figure 8. DNAPL saturation after 30 days of contaminant loading in a 50×50×100 m domain in the fracture network. Fracture CVs with low DNAPL saturation omitted.

Table 1. Mesh Data

	2D	3D Unsat.	3D Sat.
Fractures	890	230	7800
Fracture CVs	6900	31,000	200,000
Intersection CVs eliminated	2700	22,000	70,000
Porous Medium CVs	11,000	13,000	120,000
Porous Medium CVs*	23,000	80,000	15×10^6

* Count of CVs for a conventional finite volume grid.

of three simulations representing DNAPL loading in the near-surface sandstone of the Santa Susana Field Laboratory site.

The main computational advantage of the unstructured mesh over conventional grids is in the reduction of the size of the problem (i.e., number of CVs) in terms of algorithmic complexity of building and solving the numerical system of equations. Disadvantages include numerical error associated with the irregular CV connections. Many tradeoffs and computational costs regarding other implementation details (e.g., inclusion of a mobile gas phase, coupling of governing equations, field data collection and model

parameterization) are important, but shall not be discussed here.

Finally, although we have presented our CV bisection and elimination process in the context of orthogonal fractures, we believe that it could be generalized; arbitrary fracture orientations could be accommodated by a more robust fracture network generator and appropriate treatment of the permeability tensor.

ACKNOWLEDGMENTS

Funding for this project was provided by Strategic Environmental Research and Development Program, ER-1610, and subsequently by The Boeing Company via the University Consortium for Field-Focused Groundwater Contamination Research and an Industrial Research Chair grant from the Natural Sciences and Engineering Research Council of Canada.

REFERENCES

Dehotin, J., R. F. Vazquez, I. Braud, S. Debionne, and P. Viallet, Modeling of Hydrological Processes using Unstructured and Irregular Grids: 2D Groundwater Application, *J. Hydrol. Eng.*, 16 (2) 108–125, 2011.

Reitsma, S., and B. H. Kueper, Laboratory Measurement of Capillary Pressure-Saturation Relationships in a Rock Fracture, *Water Resour. Res.*, 30 (4) 865–878, 1994.

Unger, A.J.A, E. Sudicky, and P. Forsyth, Mechanisms Controlling Vacuum Extraction Coupled with Air Sparging for Remediation of Heterogeneous Formations Contaminated by Dense Nonaqueous Phase Liquids, *Water Resour. Res.*, 31 (8) 1913–1925, 1995.